Entanglement Signatures of Random Quantum Circuits

Beatriz C. Dias[1]

[1] *CeFEMA, Instituto Superior Técnico, Universidade de Lisboa, Av. Rovisco Pais, 1049-001 Lisboa, Portugal*

We study the non-equilibrium dynamics of one-dimensional quantum systems, generated by random unitary circuits, i.e. random unitary gates acting on nearest neighbour bonds. While studying different circuit models, including those formed by Haar-distributed unitaries and Clifford gates, we focus on circuits proxy to random free fermion evolution. In particular, we quantify information scrambling in the form of operator spreading for random free fermion dynamics and study the crossover from integrable-like to chaotic dynamics within random circuits. We present an exact calculation of time-ordered and out-of-time-ordered correlators measuring operator spreading for free fermion dynamics. Within this, we consider three distinct cases: the random circuit with spatio-temporal disorder (i) with and (ii) without particle number conservation and (iii) the particle non-conserving case with purely temporal disorder. In all three cases, temporal disorder causes diffusive operator spreading and $\sim \sqrt{t}$ entanglement growth. This is in sharp contrast to Anderson localization for the case of static disorder and to the ballistic behaviour observed in both the clean case of Hamiltonian evolution and in fully random unitary quantum circuits. Moreover, we perform a numerical study of the entangling properties of different circuits, with emphasis on the entanglement entropy. This numerical analysis is extended to studying the effects of adding occasional non free fermion gates (i.e. intruders) amidst free fermion circuits. We observe that this leads the initial integrable-like dynamics to become chaotic and obtain bounds on the number of intruders needed to reach the chaotic regime, which is extensive with system size.

Keywords: Random unitary circuits, out-of-time-order correlator (OTOC), diffusive operator spreading, entanglement, quantum chaos

I. INTRODUCTION

In nature, out-of-equilibrium phenomena are the rule and, in classical dynamics, they have been widely described using the theory of dynamical systems. In quantum physics though, the focus has been on the equilibrium properties of physical systems while their non-equilibrium dynamics has remained largely unaddressed. Nowadays, to understand the nature of quantum dynamics in many-body interacting systems far from equilibrium is precisely one of the central issues in physics.

Away from equilibrium, phenomena increase in complexity such that traditional many-body tools like mean-field and perturbative techniques do not apply. Removed from the sanctuary of linear response theory, one must often resort to numerical simulations, but the exponential scaling of Hilbert space dimension typically limits these to small system sizes. Even so, huge progress has been made over recent years driven partly by experiments on quantum simulators [1–4], numerical developments and occasional exact calculations. Much of this progress is associated to studying thermalization and many-body localization in quenched systems [5–9]. Moreover, the interest in features of non-equilibrium dynamics such as entanglement growth and information scrambling extends to the fields of quantum technologies and information – where the real time manipulation of interacting quantum systems is necessary to implement a quantum computer and entanglement manipulation is the underlying resource in designing efficient quantum algorithms [10] – and to high-energy physics – when studying the scrambling of information in black holes [11–13].

Random unitary circuits arise as one of the simplest and most flexible models that capture universal features in many-body dynamics, and have been intensively studied in the last few years [14–19] By mimicking time evolution by applying local random unitary gates to some underlying degrees of freedom, these allow the study of the interplay between unitarity and locality in the absence of symmetries and conservation laws. Due to the lack of much structure, these models should provide a coarse-grained description of local unitary dynamics, independent of the system's microscopic details. Although Hamiltonian dynamics and energy conservation are sacrificed, averaging over random unitary circuits respecting the symmetries of some Hamiltonian system is expected to produce results extendible to the Hamiltonian system itself. Furthermore, these circuits provide an ideal setting to perform both numerical and theoretical calculations of measures of information spreading and entanglement which characterize out-of-equilibrium time evolution.

Operator spreading and OTOC. In such circuit models, the spreading of operators can be measured by the degree to which spatially separated local operators commute after time evolution:

$$\mathcal{C}(r,t) \equiv \frac{1}{2}\mathrm{tr}\left(\rho\left[\mathcal{O}_0(t),\mathcal{O}_r\right]^\dagger\left[\mathcal{O}_0(t),\mathcal{O}_r\right]\right), \qquad (1)$$

where $\mathcal{O}_r$ is an operator localized at position r [4, 12, 13, 15–22]. The importance attached to the OTOC in random unitary circuits is that it is thought to provide a tractable instance of the physics of non-integrable many-body interacting systems, tied to thermalization and the scrambling of quantum information. Expanding $\mathcal{C} = \mathcal{C}_1 - \mathcal{C}_2$ results in a time ordered correlator $\mathcal{C}_1(r,t) = \langle\mathcal{O}_0^2(t)\mathcal{O}_r^2\rangle$ (TOC) and an out-of-time-ordered

correlator $\mathcal{C}_2(r,t) = \langle \mathcal{O}_0(t)\mathcal{O}_r\mathcal{O}_0(t)\mathcal{O}_r\rangle$ (OTOC), which behaves non-trivially. The OTOC is known to exhibit ballistic spreading and KPZ growth at the light cone interface in the simplest variant of random circuit models [15, 16] and the dynamics can be mapped to a biased random walk. In the presence of a conserved charge, this picture is modified owing to the diffusion of the conserved charges [17, 18]. Thus, one finds there is a ballistic front that itself spreads diffusively.

In addition, an exponential growth of the OTOC with a Lyapunov type exponent is thought to signal chaos [22]. Studies of information scrambling in black holes have established an upper bound for this exponent [12, 13], which is saturated in black holes and chaotic systems such as the Sachdev-Ye-Kitaev (SYK) model [23, 24].

Entanglement entropy. Another strength of random unitary circuits is in capturing entanglement growth and its saturation. Entanglement corresponds to quantum correlations without a classical counterpart. An isolated bipartition of a quantum system into subsystems A and $\bar{A}$ is entangled if it cannot be written as a product state $|\psi\rangle = |\phi^A\rangle \otimes |\varphi^{\bar{A}}\rangle$, i.e. its subsystems are not independent. This is often measured by the entanglement entropy (EE), i.e. the von Neumann entropy of the reduced density matrix ρ_A, $S = -\operatorname{tr}(\rho_A \log \rho_A)$. This is zero if A is in a pure state and higher than zero if the state is mixed. In particular, the entanglement entropy of half of the system for $|\psi\rangle$ averaged over all random pure state is $S_{\text{Page}} = L\log(2)/2 - 1/2$ (in the large L limit, with L the system size and $\dim \mathcal{H}_A = 2^{L/2}$) [25], which is lower than the maximum allowed $S_{\max} = L\log(2)/2$. For integrable (free or interacting) 1D systems and rational conformal field theories, the linear entanglement growth following a quench (i.e. the entanglement tsunami) can be understood in terms of spreading quasiparticles [26]. In numerical simulations using random unitary circuits [14] it was observed that this linear growth prior to saturation to S_{Page} is common to chaotic systems, for which the quasiparticle explanation does not hold. Instead, the EE is given by the surface of the minimal space-time membrane separating the two subsystems.

The typical linear entanglement growth prior to saturation meets some exceptions. In the presence of conserved charges, there is evidence that the Rényi entropy $S^{(2)} = -\log \operatorname{tr}\rho_A^2$ grows diffusively with $\sim \sqrt{t}$, being qualitatively different from the linear growth of the von Neumann entropy [19, 27, 28]. In many-body localized (MBL) systems, the EE grows logarithmically: $S \sim \log t$ [29, 30]. While for clean free fermion systems the quasiparticle picture and ensuing entanglement tsunami hold [26], for noisy free fermions there is evidence of diffusive growth, $S \sim \sqrt{t}$ [14, 31, 32]. Further evidence of the peculiar diffusive dynamical features of noisy free fermions is observed in the large deviation statistics of quantum expectation values and correlation functions [33, 34] and in the magnetization dynamics of the transverse field Ising model that maps to a free fermion problem [31, 35, 36].

Quantum chaos. Quantities such as the OTOC and entanglement measures should be able to distinguish between chaotic (usually highly correlated interacting systems) or non-chaotic (i.e. integrable) systems. However, for quantum systems, chaos is ill-defined; some notions of integrability are associated to classical chaos, including the amount of conserved quantities present and the existence of analytical solutions [37]. Without a standard definition, chaos is typically identified by observables serving as probes: e.g. the statistics of energy level spacings is conjectured to be Wigner-Dyson (W-D) distributed for chaotic systems and Poisson distributed for integrable-like systems.

Within the framework of random unitary circuits, the concepts of circuit complexity and pseudorandomness relate to chaos. The complexity of random circuits is measured by the notion of t-design, i.e. a subset of the unitary group $\mathrm{U}(N)$ that replicates the statistics of the first t^{th} moments of the Haar measure [38], i.e. the set X of $N \times N$ unitary matrices is a t-design if

$$\frac{1}{|X|}\sum_{U\in X} U^{\otimes t} \otimes (U^\star)^{\otimes t} = \int_{\mathrm{U}(N)} U^{\otimes t} \otimes (U^\star)^{\otimes t} dU, \quad (2)$$

with dU the Haar measure. In essence, a t-design identifies to what extent an ensemble of operators behaves like the uniform distribution on the unitary group. Chaotic systems such as black holes [11] can be well described by random models, revealing a strong connection between chaos and randomness. Furthermore, OTOCs are both a measure of chaos and circuit complexity: $2t$-point OTOCs are probes of t-designs [39]. Analogously, Rényi entropies averaged over designs of the same order are saturated to the expected chaotic value [40]. These quantities should help clarifying the gap existing between complete randomization (∞-design) and scrambling: the first implies the latter but the contrary is not true, and the latter should signal chaos.

Despite the great progress in the field of quantum dynamics, a systematic understanding of non-equilibrium phenomena is still lacking. In this work, we use random unitary circuits as toy models for the dynamics of different classes of circuits. We mainly study free fermion (FF) circuits, which first appeared as classically simulatable matchgate circuits [41], later identified as a model of free fermions in 1D [42]. Specifically, we establish through an exact calculation the diffusive behavior of $\overline{\mathcal{C}(r,t)}$ for three distinct instances of FF evolution (Section III): a particle conserving spatio-temporal random circuit (C-ST), its generalization to a non particle conserving process (NC-ST), and a spatially homogeneous case where randomness appears only in the time direction (NC-T). We also refer to numerical results for a non-conserving circuit with quenched spatial disorder (NC-S) that Anderson localizes. Besides, we review the entangling properties of not only FF circuits, but also of Haar-distributed or generic unitary (GU) and Clifford (CL) circuits (Section IV). While GU circuits mimic universal/chaotic dynamics, FF

and CL circuits are integrable-like, with the latter reproducing some features of chaotic dynamics while being classically simulatable. Finally, we obtain new results on the doping of FF circuits and the resulting crossover from integrable-like to chaotic dynamics, estimating bounds for the number of intruders necessary to reach chaos (Section V).

II. METHODS

Our system consists of a chain of L qubits (i.e. $\dim \mathcal{H}_{\text{local}} = d = 2$) realized either as spins-1/2 for GU and CL dynamics or spinless fermions for FF dynamics, evolved by applying a random unitary circuit. For GU, CL and doped FF dynamics, we must work in the many-body basis, explicitly evolving the wave function with a $2^L \times 2^L$ circuit (built out of $d^2 \times d^2$ unitaries). From this, we construct the $2^{L/2} \times 2^{L/2}$ reduced density matrix ρ_A by tracing out half of the system we then diagonalize and then we use it to compute several observables. The exponential scaling of $\dim \mathcal{H} = 2^{L/2}$ limits our numerical simulations to $L \leq 16$. However, being non-interacting, free fermions can also be described in the single particle basis such that the mean value of quadratic observables $\mathcal{O} = 1/2 A^\dagger O A$ is given by $\langle O(t) \rangle = -1/2 \operatorname{tr}(O\chi(t))$ (in particular, $S(t) = -\operatorname{tr}(\chi(t) \log \chi(t)))$ with $A = (a_0, \ldots, a_{L-1}, a_0^\dagger, \ldots, a_{L-1}^\dagger)^T$ the Nambu vector. That is, observables can be computed from the knowledge of the $2L \times 2L$ correlation matrix $\chi(t) = e^{-iHt} \chi e^{iHt}$ with $\chi = \langle A A^\dagger \rangle$, which we evolve with a $2L \times 2L$ random circuit constructed from local $2d \times 2d$ gates. This polynomial scaling with L allows us to probe much higher Ls. Let us specify the initial states, the unitaries used to built each circuit and the process of doping a circuit.

Initial state. The system is initialized in a product state $|\psi_0\rangle \otimes \cdots \otimes |\psi_{L-1}\rangle$. For FF dynamics, we have $|\Psi_1\rangle$ with each $|\psi_j\rangle$ randomly chosen to be either $|0\rangle$ or $|1\rangle$ such that the system is half-filled, i.e. $\sum_{j=0}^{L-1} n_j = \sum_{j=0}^{L-1} (\sigma_j^z + 1)/2 = L/2$, with n_j the particle number at site j and σ^z the Pauli operator. For GU and CL dynamics, the initial state is $|\Psi_2\rangle$ with $|\psi_j\rangle = \cos\theta_j |0\rangle + e^{i\phi_j} \sin\theta_j |1\rangle$ $(j = 0, \ldots, L-1)$, with θ_j and ϕ_j random real numbers in $[0, 2\pi)$. In the single particle picture for FF, we work instead with the correlation matrix initialized in $\chi = \operatorname{diag}(1 - n_1, \ldots, 1 - n_L, n_1, \ldots, n_L)$ with $(n_1, \ldots, n_L)$ a random array of 0 and 1 such that $\sum_{j=0}^{L-1} n_j = L/2$.

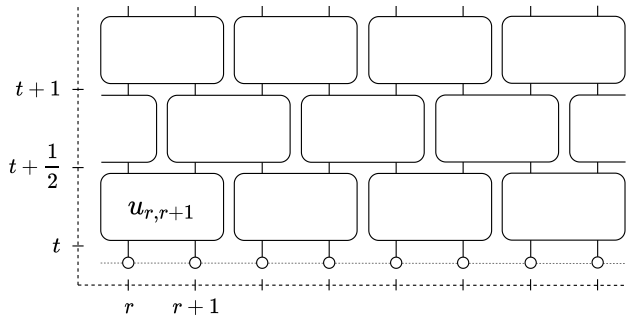

FIG. 1. Quantum circuit acting on L sites (horizontal axis). At each time step (vertical axis), unitaries $u_{r,r+1}$ are chosen randomly from some set and applied to neighbouring sites r and $r+1$. At integer and half-integer time steps, these are respectively applied to even $(2R, 2R+1)$ and odd $(2R, 2R+1)$ pairs of sites, with $R = 0, \ldots, L/2 - 1$. Due to periodic boundary conditions, the sites are modulo L.

Random unitary circuits. The unitary circuit acts on a chain of L sites $(r = 0, ..., L-1)$ and periodic boundary conditions as a discrete time protocol, following the brick wall pattern shown in Fig. 1. In the many-body picture, a time step corresponds to the action of the unitary operation $\mathcal{U} = \mathcal{U}_{\text{even}} \mathcal{U}_{\text{odd}}$, obtained by the successive application of the half-steps $\mathcal{U}_{\text{even}} = \bigotimes_{R=0}^{L/2-1} \mathcal{U}_{2R,2R+1}$ and $\mathcal{U}_{\text{odd}} = \bigotimes_{R=0}^{L/2-1} \mathcal{U}_{2R-1,2R}$. Here, $\mathcal{U}_{r,r+1}$ is a random unitary acting nontrivially on the local 4-dimensional Hilbert space of sites r and $r+1$. Random unitary circuits built using two-site unitaries respecting different symmetries lead to different dynamics: GU, CL and FF (which includes NC-ST, C-ST, NC-T and NC-S). For GU evolution, $\mathcal{U}_{r,r+1}$ are sampled over U(4) according to the Haar-measure [14], which can be done using Python's algorithm `scrip.stats.unitary_group.rvs(N)` [43]. The Clifford group is generated by $\{\text{CNOT}_\text{L}, \text{H}, \text{P}\}$ [44], i.e. the two-site controlled NOT gate, CNOT_L (which flips the second bit if the first one is 1), the single-site Hadamard, H (a rotation of π on the Bloch sphere around the $(1, 0, 1)$ axis), and the single-site phase gate, P (which adds a phase $e^{i\pi/4}$ if the bit is 1). Thus, for CL evolution we consider $\mathcal{U}_{r,r+1} = C \cdot (B \otimes A)$, with A and B randomly chosen from $\{\mathbb{1}_2, \text{H}, \text{P}\}$ and C from $\{\mathbb{1}_4, \text{CNOT}_\text{L}, \text{CNOT}_\text{R}\}$ (to increase the generation of entanglement, we included the CNOT with the control bit on the right, i.e. CNOT_R).

For FF dynamics, the evolution operator must leave invariant the algebra of single-particle fermionic creation and annihilation operators ($a_r^\dagger$ and a_r) [41, 42], i.e. $\mathcal{U}_{r,r+1}^\dagger A_r \mathcal{U}_{r,r+1} = u_{r,r+1} A_r$, where $A_r = (a_r, a_{r+1}, a_r^\dagger, a_{r+1}^\dagger)^T$ and $u_{r,r+1}$ is a 4×4 unitary matrix respecting particle-hole (PH) symmetry, i.e. $\tau_1 u_{r,r+1}^T \tau_1 = u_{r,r+1}^\dagger$, with τ_1 a Pauli matrix acting on Nambu space. These single-particle operators obeying PH symmetry can be realized as $u_{r,r+1} = V^\dagger O V$, with $V = 1/\sqrt{2} \begin{pmatrix} \mathbb{1} & \mathbb{1} \\ -i\mathbb{1} & i\mathbb{1} \end{pmatrix}$ and O a Haar-distributed orthogonal matrix, which can be obtained using Python's algorithm `scipy.stats.unitary_ortho.rvs(4)` [43]. The gates can be translated to the many body $\mathcal{U}_{r,r+1}$ [41, 42] using the Wigner-Jordan transformation [45]. While for NC-ST each $u_{r,r+1}$ is randomly generated, for NC-T at each time step the same unitary is applied to all pairs of sites, i.e. $u_{r,r+1} = u$, and for C-ST $u_{r,r+1} = v_{r,r+1} \oplus v_{r,r+1}^*$, with $v_{r,r+1}$ a 2×2 Haar-distributed unitary matrix.

Doping. Doping is understood as the application of occasional gates belonging to a different set (i.e. intruder

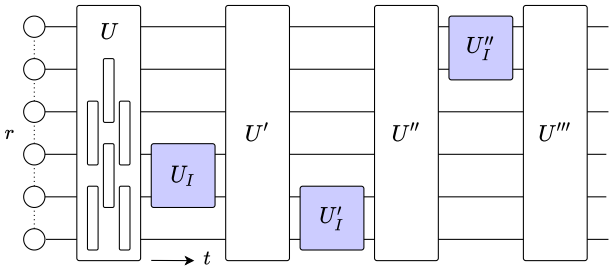

FIG. 2. Starting from an initial product state, the main FF circuits $U, U', \ldots$ built using two-site unitaries, as shown in Fig. 1, are interleaved with two-site intruders $U_I, U'_I, \ldots$ applied to randomly chosen pairs of sites. The main circuits have enough depth Δt such that the system stabilizes (i.e. S plateaus) before applying the next intruder

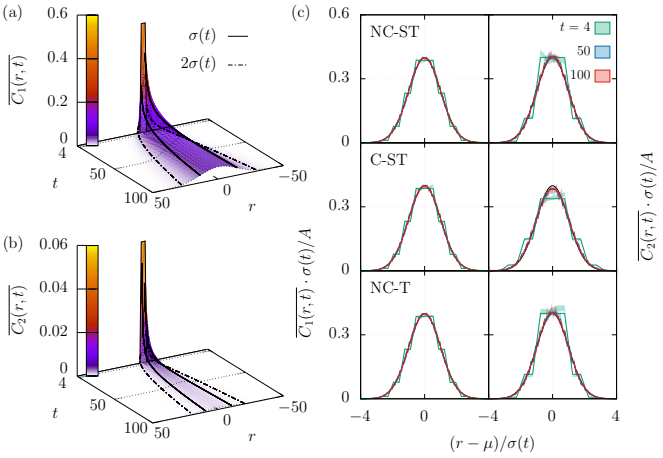

FIG. 3. (a) and (b) Exact $\overline{\mathcal{C}_1(r,t)}$ and $\overline{\mathcal{C}_2(r,t)}$ for a system with 100 sites, for NC-ST (and NC-T) evolution. The black curves envelop the $\sigma(t)$ and $2\sigma(t)$, with $\sigma(t) = \sqrt{2t}$ for $\overline{C_1}$ and with $\sigma(t) = \sqrt{t}$ for $\overline{C_2}$. (c) Rescaled TOC (left) and OTOC (right), i.e. $\overline{C_1(r,t)}\,\sigma(t)/A$ and $\overline{C_2(r,t)}\,\sigma(t)/A(t)$ (with A the normalization), as a function of $(r-\mu)/\sigma(t)$ for $t \in \{4, 50, 100\}$ and for NC-ST (top), CS-T (middle) and NC-T (bottom). Full lines correspond to exact calculations (shown in (a) and (b) for NC-ST) and the color filled region to simulations including an average over 4000 disorder realizations, starting from a random product state with particle number fixed to $L/2$. Both collapse to the continuum limit solution, i.e. $g(r,t) = 1/(\sqrt{2\pi})\exp[-(r-\mu)^2/(2\sigma^2(t))]$. For $\overline{C_1(r,t)}$, $A = 2$ and $\sigma(t) = \sqrt{2t}$ for all cases; for $\overline{C_2(r,t)}$, $\sigma(t) = \sqrt{t}$ for all cases, $A(t) = 1/(2\sqrt{2\pi t})$ for NC-ST and NC-T and $A(t) = 2/(\sqrt{2\pi t})$ for C-ST. The deviation $\mu = 1/2$ centers $\overline{C_1}$ and $\overline{C_2}$ around $r = 0$.

gates) amidst some underlying dynamics. In particular, an initial state is evolved by applying a random quantum circuit with depth Δt (i.e. with Δt bilayers) built as usual with two-site FF gates; after the system stabilizes, a two-site non free fermion gate is applied to a randomly chosen pair of sites. This procedure is repeated N_I times, as seen in Fig. 2. We average over several realizations.

We consider as intruders: random Haar-distributed unitary gates $\in U(4)$ (GU) and a fixed CL gate given by $\mathrm{CNOT_L} \cdot (\mathrm{H} \otimes \mathbb{1}_2)$ (CL). In the spirit of studying the simplest extension of FF to an interacting model, we also consider $\mathrm{ZZ}_{r,r+1} = \exp(-i\frac{\pi}{4}\sigma^z_r \otimes \sigma^z_{r+1})$ ($\mathrm{ZZ}_{\pi/4}$ intruders), which account for terms of the type $a^\dagger_r a_r a^\dagger_{r+1} a_{r+1}$. Besides, we consider the particle number conserving case analogous to FF circuits (CFF) injected with GU intruders. Conserving GU (CGU) unitaries are $U_C = e^{iq_0} \oplus Q_1 \oplus e^{iq_2}$, with q_0 and q_2 random numbers in $[0, 2\pi)$ and Q_1 a Haar-distributed 2×2 unitary matrix.

The different types of dynamics are labelled as 'main circuit : intruders', e.g. FF : GU stands for FF circuits doped with GU gates. Occasionally, we identify the initial state through a subscript, e.g. $\mathrm{FF}_{|\Psi_1\rangle}$.

III. OPERATOR SPREADING AND OTOC

An analytical expression for the OTOC averaged over disorder for evolution under generic unitary circuits was obtained by Nahum *et al.* in Ref. [15]. We present equivalent analytical results for three instances of free fermion evolution: C-ST, NC-ST and NC-T. The time-ordered density-density correlator $\langle O_0(t) O_r \rangle$ becomes trivial when averaged over temporal disorder [46], but $\mathcal{C}(r,t)$, given by (1), remains non-trivial upon averaging. We consider an average over separable initial states, which is equivalent to taking $\rho \propto 1$ in (1), i.e. the infinite temperature ensemble. In the following, we shall consider quadratic observables $\mathcal{O}_r = 1/2 A^\dagger O_r A$ where O_r is a local single-particle operator. The computation of $\mathcal{C}(r,t)$ for free fermions can be brought into a form where the trace need only be performed over $2L \times 2L$ matrices rather than over the entire Hilbert space. One can show that the many-body correlator can be written in terms of single-body quantities as $\mathcal{C}(r,t) = 1/2^3[C_1(r,t) - C_2(r,t)]$, where

$$C_1(r,t) = \mathrm{tr}\left[O_0^2(t) O_r^2\right], \tag{3}$$

$$C_2(r,t) = \mathrm{tr}\left[O_0(t) O_r O_0(t) O_r\right], \tag{4}$$

and $O(t) = UO(t-1)U^\dagger$. The general relation between the single particle and many-body TOC and OTOC is given in Ref. [46].

Numerics of TOC and OTOC. The TOC (C_1) and OTOC (C_2) may now be simulated efficiently by generating local pseudo-random gates $u_{r,r+1}$, as described in Section II, and averaging the result over many realizations of the time evolution. Results for $L = 100$ are shown in Fig. 3(c) for a symmetrized particle number operator $\mathcal{O}_r = 1/2(a^\dagger_r a_r - a_r a^\dagger_r) = a^\dagger_r a_r - 1/2$. In contrast to the ballistic spreading seen in Haar-random circuits, $\overline{\mathcal{C}(r,t)}$ diffuses for random free fermions. This can be seen most clearly in Fig. 3(c) where $\overline{C_1}\,\sigma(t)/A$ and $\overline{C_2}\,\sigma(t)/A(t)$ are shown to collapse to a Gaussian with standard deviation growing respectively with $\sqrt{2t}$ and $\sqrt{t}$ at multiple fixed times, with the horizontal axis rescaled to $(r-\mu)/\sigma(t)$. Both the ordinary two-time correlator $\overline{C_1}$ and the true

out-of-time order component $\overline{C_2}$ are diffusive. The magnitude of $\overline{C_1}$ is, however, much larger than that of $\overline{C_2}$ at fixed time. These results are compatible with the $\sim\sqrt{t}$ early time entanglement growth observed in Section IV.

Exact calculation of $\overline{C_1(r,t)}$. We now look for the origin of the diffusive behavior of $\overline{\mathcal{C}(r,t)}$ examining $\overline{C_1(r,t)}$ and $\overline{C_2(r,t)}$ in turn and proceeding analytically by computing the exact averages over the random unitaries for the NC-ST case, referring to Ref. [46] for further details. In the single particle picture, we may denote states of the system by $|\alpha\rangle \equiv |r_\alpha, s_\alpha\rangle \equiv |2R_{r_\alpha}+b_\alpha, s_\alpha\rangle$, where $r_\alpha = 0,\dots,L-1$ runs over the sites, $s_\alpha \in \{p,h\}$ labels the particle-hole index; $R_{r_\alpha}=0,\dots,L/2-1$ labels the pair of sites $(r_\alpha, r_\alpha+1)$ and $b_{r_\alpha}\in\{0,1\}$ such that $r_\alpha = 2R_{r_\alpha}+b_{r_\alpha}$. Note that the sites are acted upon by modulo L, due to periodic boundary conditions.

Starting with $\overline{C_1(r,t)}$ given by (3), we use a notation in which operators are rendered as state vectors $C_1(r,t) = \mathrm{tr}\left[O_0^2(t)O_r^2\right] = \langle\langle O_r^2||\, O_0^2(t)\rangle\rangle$, where $||O_r^2\rangle\rangle \equiv ||O_r^2(0)\rangle\rangle$, $||O_r^2(t)\rangle\rangle = \sum_{\alpha\beta}||\alpha\beta\rangle\rangle\langle\alpha|O_r^2(t)|\beta\rangle$ and $||\alpha\beta\rangle\rangle = |\alpha\rangle\otimes\langle\beta|^T$. With O_r the symmetrized number operator, we get $||O_r^2\rangle\rangle = \sum_s ||r,s;r,s\rangle\rangle$. For a single realization, $O_0^2(t+1) = U^\dagger O_0^2(t)U$, which translates to $||O_0^2(t+1)\rangle\rangle = U^\dagger\otimes U^T\,||O_0^2(t)\rangle\rangle$. Applying one layer of the circuit, i.e. $U = U_{\mathrm{even}}U_{\mathrm{odd}}$, and averaging over multiple realizations of the random circuit as summarized in Ref. [46] one finds

$$||\overline{O_0^2(t+1)}\rangle\rangle = \hat{W}_1\,||\overline{O_0^2(t)}\rangle\rangle \tag{5}$$
$$\hat{W}_1 \equiv \left[\sum_{R=0}^{L/2-1}||\phi_{2R}\rangle\rangle\langle\langle\phi_{2R}||\right]\left[\sum_{R=0}^{L/2-1}||\phi_{2R-1}\rangle\rangle\langle\langle\phi_{2R-1}||\right],$$

having introduced

$$||\phi_r\rangle\rangle \equiv \frac{1}{2}\sum_{x\in\{r,r+1\}}\sum_s ||x,s;x,s\rangle\rangle\,. \tag{6}$$

With the initial condition $||\overline{O_0^2(0)}\rangle\rangle = \sum_s||0,s;0,s\rangle\rangle$, the time evolution of $\overline{C_1}$ is completely determined. The subspace spanned by $||\phi_r\rangle\rangle$ is closed under the evolution thus respecting the particle-hole symmetry. These vectorized operators obey $\langle\langle\phi_r\,||\phi_{r'}\rangle\rangle = \delta_{r',r}+\frac{1}{2}\delta_{r',r\pm1}$, that leads the recursion relation (5) to be simplified to

$$\left\langle\langle\phi_r\,\middle\|\,\overline{O_0^2(t+1)}\right\rangle\right\rangle = \frac{1}{4}\Big(\langle\langle\phi_{r-2}|| + 2\langle\langle\phi_r|| + \langle\langle\phi_{r+2}||\Big)\,||\overline{O_0^2(t)}\rangle\rangle\,. \tag{7}$$

From this and the initial condition we obtain

$$\overline{C_1(2R,t+1)} = \overline{C_1(2R+1,t+1)} = \frac{1}{4}\Big(\overline{C_1(2R-2,t)} + 2\overline{C_1(2R,t)} + \overline{C_1(2R+2,t)}\Big) \tag{8}$$

for $t\geq 1$ and $\frac{1}{2}(\delta_{R-1,0}+\delta_{R,0})$ for $t=0$ – this exact result is pictured in Fig. 3(a). This tells us that $\overline{C_1(r,t)}$ is equivalent to an average over all possible classical random walks respecting the geometry of the circuit: tarting from $\overline{C_1(r,t=0)} = 2\delta_{r,0}$, each weight $\overline{C_1(r,t)}$ is divided among its nearest neighbours $\overline{C_1(r-1,t+1/2)}$ and $\overline{C_1(r+1,t+1/2)}$.

Taking the continuum limit, $\lim_{t,L\to\infty}\overline{C_1(r,t)} = \lim_{a\to0} a\overline{C_1'(x=ra,\tau=ta^2)}$, we recover the 1D diffusion equation $\partial_\tau\overline{C_1'(x,\tau)} = \partial_x^2\overline{C_1'(x,\tau)}$ with diffusion constant $D=1$ which approximates the exact discrete evolution very well, even for relatively small times (see Fig. 3(c)).

Exact calculation of $\overline{C_2(r,t)}$. The calculation of $\overline{C_2(r,t)}$ proceeds analogously to that of $\overline{C_1(r,t)}$ but is more involved not least because the disorder average is carried out over a product of four unitaries rather than two in the case of $\overline{C_1}$. As before, we write the correlator (4) in a vectorized notation

$$C_2(r,t) = \mathrm{tr}\left[O_0(t)O_rO_0(t)O_r\right] = \langle\langle Q_r||\,S\,||Q_0(t)\rangle\rangle\,, \tag{9}$$

with $Q_r \equiv O_r\otimes O_r$ fixed by the choice of observable to

$$||Q_r\rangle\rangle = \sum_s ||rs,rs,rs,rs\rangle\rangle - ||rs,r\bar{s},rs,r\bar{s}\rangle\rangle\,, \tag{10}$$

with $s=p,h$ and the corresponding $\bar{s}=h,p$ and

$$||Q_r(t)\rangle\rangle = \sum_{\alpha\beta\mu\nu}||\alpha\beta\mu\nu\rangle\rangle\langle\alpha\beta|Q_r(t)|\mu\nu\rangle\,, \tag{11}$$
$$S = \sum_{\alpha\beta\mu\nu}||\alpha\beta\mu\nu\rangle\rangle\langle\langle\alpha\beta\nu\mu||\,, \tag{12}$$

where $||\alpha\beta\mu\nu\rangle\rangle = |\alpha\beta\rangle\otimes\langle\mu\nu|^T$. The state $||Q_0(t)\rangle\rangle$ evolves as

$$||Q_0(t+1)\rangle\rangle = U^\dagger\otimes U^\dagger\otimes U^T\otimes U^T\,||Q_0(t)\rangle\rangle \tag{13}$$

and an average is taken over different realizations eventually leading to the recursion relation

$$\left\langle\langle\Theta\bar{\Theta}_{r,r'}\,\middle\|\,\overline{Q_0(t+1)}\right\rangle\right\rangle = \hat{W}_2\,||\overline{Q_0(t)}\rangle\rangle\,, \tag{14}$$

$$\hat{W}_2 \equiv \mathrm{tr}\left[\boldsymbol{M}_{r,r'}\boldsymbol{\Upsilon}_{r,r'}\right],$$
$$\boldsymbol{\Upsilon}_{r,r'} \equiv \begin{pmatrix}\langle\langle\Theta\bar{\Theta}_{r-2,r'-2}|| & \langle\langle\Theta\bar{\Theta}_{r-2,r'}|| & \langle\langle\Theta\bar{\Theta}_{r-2,r'+2}||\\ \langle\langle\Theta\bar{\Theta}_{r,r'-2}|| & \langle\langle\Theta\bar{\Theta}_{r,r'}|| & \langle\langle\Theta\bar{\Theta}_{r,r'+2}||\\ \langle\langle\Theta\bar{\Theta}_{r+2,r'-2}|| & \langle\langle\Theta\bar{\Theta}_{r+2,r'}|| & \langle\langle\Theta\bar{\Theta}_{r+2,r'+2}||\end{pmatrix},$$

analogous to (7). In the above expression, $\boldsymbol{M}_{r,r'}$ are 3×3 matrices of constant coefficients given explicitly in Ref. [46]: there are four distinct $\boldsymbol{M}_{r,r'}$ for $r' = r, r\pm2, r\pm4$ and one for all remaining r'. Also,

$$||\Theta\bar{\Theta}_{r,r'}\rangle\rangle = ||\Theta_{r,r'}\rangle\rangle - ||\bar{\Theta}_{r,r'}\rangle\rangle\,, \tag{15}$$

and

$$||\Theta_{r,r'}\rangle\rangle = \frac{1}{\sqrt{g_{r,r'}}}\sum_{\substack{r_\alpha\in\{r,r+1\}\\ r_\beta\in\{r',r'+1\}}}\sum_{s_\alpha,s_\beta}||\alpha\beta\beta\alpha\rangle\rangle\,, \tag{16}$$
$$||\bar{\Theta}_{r,r'}\rangle\rangle = \frac{1}{\sqrt{g_{r,r'}}}\sum_{\substack{r_\alpha\in\{r,r+1\}\\ r_\beta\in\{r',r'+1\}}}\sum_{s_\alpha,s_\beta}||\alpha\bar{\alpha}\beta\bar{\beta}\rangle\rangle\,, \tag{17}$$

with $g_{r,r'} = N(N-\delta_{r,r'})$. This completely determines the evolution of the single particle OTOC. With the initial condition (10), one finds

$$\overline{C_2(r,t=0)} = 2\delta_{r,0}, \tag{18}$$

$$\overline{C_2(r,t=1)} = \frac{1}{18}\left(\delta_{r,-1}+\delta_{r,0}\right), \tag{19}$$

and, for subsequent times, we define

$$K_{r,r'}(t) \equiv \frac{1}{2\sqrt{3}}\Big\langle\Big\langle \Theta\bar{\Theta}_{r,r'}\Big\|\overline{Q_0(t)}\Big\rangle\Big\rangle, \tag{20}$$

and use (14) to get $\overline{C_2(2R,t+1)} = \overline{C_2(2R+1,t+1)} = \mathrm{tr}\left[\boldsymbol{M}_{2R,2R'}\boldsymbol{K}_{2R,2R'}(t)\right]$ with

$$\boldsymbol{K}_{2R,2R'}(t) \equiv \begin{pmatrix} K_{2R-2,2R'-2} & K_{2R-2,2R'} & K_{2R-2,2R'+2} \\ K_{2R,2R'-2} & K_{2R,2R'} & K_{2R,2R'+2} \\ K_{2R+2,2R'-2} & K_{2R+2,2R'} & K_{2R+2,2R'+2} \end{pmatrix}. \tag{21}$$

The evolution thus described exactly is pictured in Fig. 3(b) and it reproduces the numerical results seen in Fig. 3(c). Let us highlight one important distinction between $\overline{C_1}$ and $\overline{C_2}$: while $\overline{C_1}$ is a 1D diffusive process, the evolution of $\overline{C_2}$ is given by the diagonal of $\boldsymbol{K}_{2R,2R'}(t)$, which diffuses in 2D. Analogously to $\overline{C_1}$, the bulk behaviour of $\boldsymbol{K}_{2R,2R'}(t)$ can be described by an average over all possible classical random walks, but in 2D.

In the continuum limit, $\overline{C_2(r,t)} = \lim_{a\to 0}\overline{C_2'(x=ra,\tau=ta^2)} \simeq fa^2K'_{x,x'}(\tau)$, where $K'_{x,x'}(\tau)$ can be shown to obey the 2D diffusion equation $\partial_\tau K'_{x,x'}(\tau) = \left(\partial_x^2+\partial_{x'}^2\right)K'_{x,x'}(\tau)$ with initial condition $K'_{x,x'}(0) = 2\delta(x)\delta(x')$ and $f = 1/2$ for NC-ST [46]. Note that $\lim_{t\to\infty}\overline{C_2(r,t)}/\overline{C_1(r,t)} = 0$, i.e. for large times the $\overline{C_1(r,t)}$ dictates the leading behavior of the OTOC.

Extensions to C-ST, NC-T and NC-S. We have shown that both $\overline{C_1}$ and $\overline{C_2}$ spread diffusively for free fermions in 1D in the presence of spatio-temporal noise (NC-ST). In Ref. [46] we lay out equivalent exact calculations of $\overline{C_1}$ and $\overline{C_2}$ for two further cases: C-ST which conserves the particle number and NC-T where the unitary evolution is spatially homogeneous but has temporal noise. The result is that there is diffusive spreading in all three cases. The space translation invariance in NC-T lifts some restrictions in the dynamics such that $\overline{C_1(r,t)}$ and $\overline{C_2(r,t)}$ could arise respectively from 2D and 4D processes, but the initial diagonal observables reduce the exact expressions to the 1D (8) and 2D (21) processes known for NC-ST. Regarding C-ST, although the absence of anomalous terms leads to a different exact expression for $\overline{C_2}$, such that its normalization in the continuum limit differs is $f = 2$ instead of $f = 1/2$, it preserves its diffusive behaviour.

In contrast, numerical results obtained for the temporal homogeneous case (NC-S) in Ref. [46], where even and odd layers of random gates are fixed and applied repeatedly in time, show that $\overline{C_1}$ and $\overline{C_2}$ remain Anderson localized [47], decaying exponentially around $r = 0$.

IV. DYNAMICS OF ENTANGLEMENT

For completeness, we characterize the growth of entanglement in the different circuits (FF, CL and GU), as measured by the entanglement entropy. Other entanglement measured such as the statistics of energy level spacings (which exhibit level repulsion for chaotic, but not for integrable-like dynamics) are shown in Ref. [46]

We start by analysing the dynamics of the von Neumann entropy, $S = -\,\mathrm{tr}(\rho_A \ln \rho_A)$, with ρ_A the reduced density matrix of a subsystem of size $L/2$, starting from an initial product state with a well defined particle number. For FF dynamics, Fig. 4(b) shows that, for all three cases NC-ST, C-ST and NC-T, the entanglement grows as $\sim D_S\sqrt{t}$ for small times (with D_S a time independent constant), saturating at times $t_{\mathrm{sat}} \sim L^2$. Asymptotically

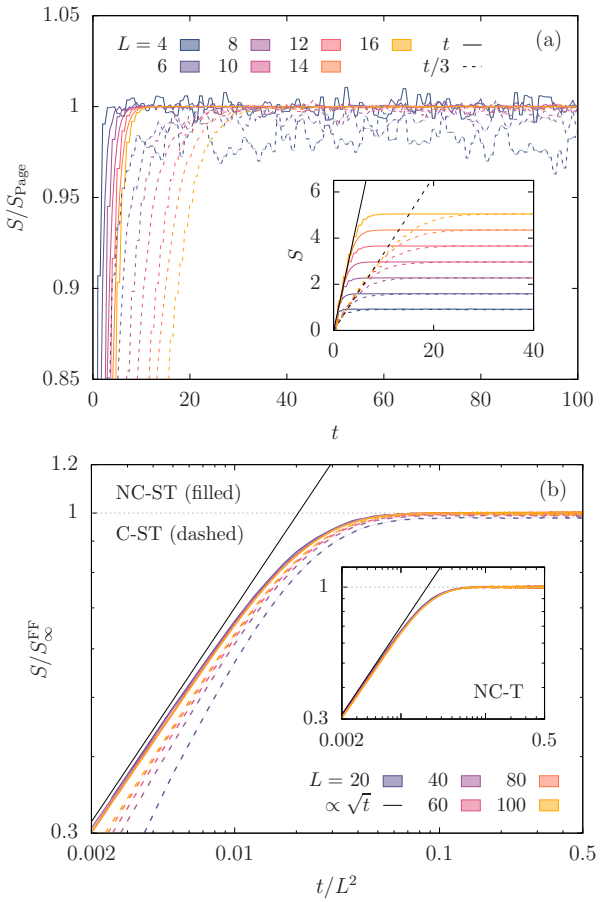

FIG. 4. (a) Time series of the entanglement entropy divided by the Page value S/S_{Page} for GU (filled) and CL (dashed) dynamics and $L \in \{4,6,\ldots,14,16\}$. In the inset, we plot the non-rescaled $S(t)$. The data is an average over 1000 realizations (450 for $L = 16$), starting from a random product state.(b) Growth of the entanglement entropy divided by the saturation value S/S_∞^{FF} as a function of t/L^2 for random free fermions − NC-ST (filled), C-ST (dashed) and NC-T (inset) − with $L = 100$, showing $S(t) \propto \sqrt{t}$ at the earliest times. The curves for NC-ST and NC-T overlap.

diffusive growth of the Rényi entropy $S^{(2)}$ has been discussed in the literature, coinciding with linear growth of the von Neumann entropy at least in low dimensional local Hilbert spaces in models with conserved quantities [19, 27, 48]. The random circuit free fermion model is therefore qualitatively different to these cases. For $t \gg t_{\rm sat}$, the saturation value $S_\infty^{\rm FF} = s_0 L + s_1 + O(1/L)$, coincides with the mean entanglement entropy of a random Gaussian state [49–52], with $s_0 \simeq 0.193$ for all the considered free fermion processes and $s_1 \simeq 0.085$ for the NC-ST case, well below the Page value ($s_0 = \ln 2/2 \simeq 0.346, s_1 = -1/2$) obtained by averaging over the full Hilbert space [25]. These results show that the rate of increase of the entanglement is compatible with diffusion of quantum information. In addition, while the saturation entanglement has volume law scaling, free fermion dynamics cannot explore the full Hilbert space.

In Fig. 4(a), despite the small L, we see the expected initial linear growth of $S(t)$ for evolution under GU circuits, which saturates at $S_{\rm Page}$ [25]. This is replicated using CL dynamics, with small deviations from $S_{\rm Page}$ occurring for small L and, overall, higher fluctuations being present.

V. DOPED FREE FERMION CIRCUITS

Here, we propose to investigate the emergence of chaos when doping integrable-like free fermion circuits, as described in Section II. In particular, we study how different observables (or probes) explore random matrix behaviour (in the sense that they reach the values expected for GU circuits) as intruders are applied, which we interpret as chaos. By studying the dependence of the different probes on N_I and L, we obtain bounds on the number of intruders N_I needed to obtain a (good enough) approximation of chaos. Since we are restricted to simulate small system sizes, this is done by extending the finite size scaling analysis to the thermodynamic limit.

Probes of chaos. We see chaos ensuing as the probes we use approach the expected values for chaotic dynamics (obtained with GU circuits). We consider the following probes, P: the mean and fluctuations of the entanglement entropy, $S = -\operatorname{tr}(\rho_A \log \rho_A)$, and of the 2$^{\rm nd}$ Rényi entropy, $S^{(2)} = -\log \operatorname{tr}(\rho_A^2)$; the fluctuations of the particle number of half of the system, $n_{\rm half} = \sum_{j=0}^{L/2-1} n_j$, and also the mean of the 'normalized' ratio of level spacings $\tilde{r}$, i.e. $\tilde{r}_n = \min(s_n/s_{n-1}, s_{n-1}/s_n)$, with $s_n = e_{n+1} - e_n$ and e_n the ordered eigenvalues of $-\log \rho_A$, which serves as an effective Hamiltonian. The mean values are $\mu(P) = 1/N \sum_{i=1}^N P_i$, while the fluctuations are measured by the variance $\sigma^2(P) = \frac{1}{N-1} \sum_{i=1}^N (P_i - \mu(P))^2$, with N the number of points and P_i the $i^{\rm th}$ point.

The extent to which these probes reach the chaotic values can be made precise using more or less restrictive criteria. We consider that (a good enough approximation of) chaos is achieved when the mean measures reproduce the values expected for GU dynamics within their typical fluctuations, i.e. when

$$F_\mu(\#) = \frac{|\mu(\#)(N_I, L) - \mu(\#_{\rm GU})|}{\sigma(\#_{\rm GU})} \leq \mathcal{O}(1), \qquad (22)$$

with $\# = S$ or $S^{(2)}$; or, using the criterion of Ref. [53] for fluctuations, when

$$F_{\sigma^2}(\#) = \frac{|\sigma^2(\#)(N_I, L) - \sigma^2(\#_{\rm GU})|}{\sigma^2(\#_{\rm GU})} \leq \mathcal{O}(1), \qquad (23)$$

with $\# = S, S^{(2)}$ or $n_{\rm half}$, where the dependence of the GU values on L is omitted.

Results. Each probe $P(t)$ usually rises (or diminishes) in time in well defined plateaus: after each intruder is applied, it quickly rises (or diminishes) to stabilize at some value, as seen in Fig. 5 for $\mu(S)$ and $\sigma^2(S)$ for FF : GU dynamics. Take $P(N_I, L)$ to be the value of the probe P taken at the plateau following the injection of N_I intruders for a system with L sites. This again rises (or diminishes, depending on whether $P = \mu(\#)$ or $P = \sigma^2(\#)$) from $P(0, L)$ to $P(\infty, L)$ with some function $f(N_I, L)$ decaying to zero, i.e. $P(N_I, L) = P(\infty, L) + [P(0, L) - P(\infty, L)] f(N_I, L)$, where $P(\infty, L) \approx P_{\rm GU}$ for almost all the cases studied. Our numerical results, shown in Fig. 6 for $\mu(S)$ and $\mu(S^{(2)})$ for FF dynamics doped with GU intruders (equivalent pictures for the remaining cases in Ref. [46]), suggest that $f(N_I, L) \approx e^{-g(L) N_I}$, at least in the long-time or large N_I regime (in some cases, namely CFF : CGU, some deviations occur for small N_I). Furthermore, at least in the range of Ls probed (apart from deviations occurring for small L), the exponent seems to be well approximated by $g(L) \approx \beta L^{-\alpha}$, with α and β constants dependent on the underlying dynamics and the type of intruders. Thus, we consider

$$\begin{aligned} Q(P) &\equiv Q(P(N_I, L)) \\ &= \frac{P(N_I, L) - P(\infty, L)}{P(0, L) - P(\infty, L)} \approx \gamma e^{-\beta L^{-\alpha} N_I}, \end{aligned} \qquad (24)$$

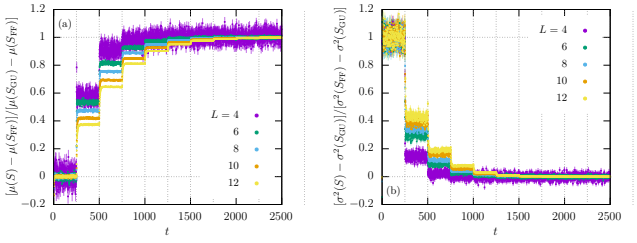

FIG. 5. (a) Time series of the mean EE rescaled according to $[\mu(S) - \mu(S_{\rm FF})]/[\mu(S_{\rm GU}) - \mu(S_{\rm FF})]$ so that it varies from 0 to 1. (b) Time series of the fluctuations of the EE rescaled as $[\sigma^2(S) - \sigma^2(S_{\rm GU})]/[\sigma^2(S_{\rm FF}) - \sigma^2(S_{\rm GU})]$ so that it drops from 1 to 0. This is shown for FF dynamics doped with GU intruders every $\Delta t = 250$ (vertical lines), for $L \in \{4, 6, 8, 10, 12\}$. The system is initialized in a product state and the data is an average over 1000 realizations (4000 for $L = 4$).

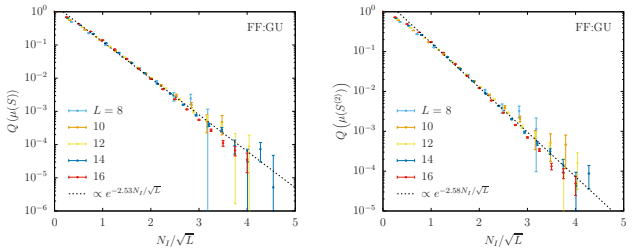

FIG. 6. Plateau values of $\mu(S)$ and $\mu(S^{(2)})$ rescaled as $Q(P) = [P(N_I, L) - P(\infty, L)]/[P(0, L) - P(\infty, L)]$, with $P = \mu(S), \mu(S^{(2)})$, as a function of N_I/L^α up to $L = 16$, where α is given in Tab. I, for FF : GU dynamics. Note that $P(\infty, L) = P_{\rm GU}$ and $N_{I_{\rm tot}} = 20$. Each point associated to N_I is taken in the plateau following the application of N_I gates and is an average over 4000 realizations (3000 for $L = 16$). The expression $\gamma \exp(-\beta L^{-\alpha} N_I)$ was fitted to the data.

main + intruders → ensuing dynamics	$\mu(S)$	$\mu(S^{(2)})$	$\sigma^2(S)$	$\sigma^2(S^{(2)})$	$\sigma^2(n_{\rm half})$
CL : T → GU	sat	sat	0	0	sat
CL : GU → GU	sat	sat	0	0	sat
FF : GU → GU	1/2	1/2	1/4	1/4	1/4
FF : CL → GU	1/2	1/2	−−	−−	−−
CFF : CGU → CGU	1	1	1	1	1
$\mathrm{FF}_{\vert\Psi_1\rangle}$: $\mathrm{ZZ}_{\pi/4}$ → new	1	1	1/2	1/2	1
$\mathrm{FF}_{\vert\Psi_2\rangle}$: $\mathrm{ZZ}_{\pi/4}$ → GU	1	1	1/2	1/2	1

TABLE I. Values of α such that $\gamma \exp(-\beta L^{-\alpha} N_I)$ fits the data $Q(P)$, which rescales P to diminish from 1 to 0, as defined in (24), where P is $\mu(S)$, $\mu(S^{(2)})$, $\sigma^2(S)$, $\sigma^2(S^{(2)})$ or $\sigma^2(n_{\rm half})$. This is shown for the different types of main circuit + intruders studied. This can be seen visually in Fig. 6 and in Ref. [46]. Entries with '−−' correspond to cases not studied, while 'sat' indicates that $P(N_I = 0)$ is already saturated to $P(N_I \to \infty)$.

which drops from 1 to 0. Being an exponential law, this suggests that the rate of decrease of $P(N_I, L) - P(\infty, L)$ depends on the fraction of the interval $P(0, L) - P(\infty, L)$ left to undergo.Besides, it indicates that $N_I \sim \mathcal{O}(L^\alpha)$ intruders are necessary to undergo some fraction of the transition from $P(0, L)$ to $P(\infty, L)$. Note that this fixed relative error is less restrictive than the conditions for chaos (22) and (23).

For the different probes and dynamics studied, having fixed the N_I dependence in $\gamma \exp(-\beta L^{-\alpha} N_I)$, we find the α among integers and half-integers (and also 1/4) that best suits the data (see Tab. I). This is done by visual inspection of Fig. 6 and of the remaining figures in Ref. [46].

Knowing α which controls the scaling of (24) with L (see Tab. I), we can find bounds on N_I respecting the conditions for chaos (22) and (23). For $\# = S$ and $S^{(2)}$, we can use (24) and $[\mu(\#)(0, L) - \mu(\#)(\infty, L)]/\sigma(\#)(\infty, L) \sim \mathcal{O}(L)\, e^{\mathcal{O}(L)}$ [46] to show that

$$F_\mu(\#) = \frac{\mu(\#)(0, L) - \mu(\#)(\infty, L)}{\sigma(\#)(\infty, L)} Q(\mu(\#)) \sim \mathcal{O}(L)\, e^{\mathcal{O}(L)} e^{-\mathcal{O}(L^{-\alpha} N_I)}. \quad (25)$$

Also, for $\# = S, S^{(2)}$ or $n_{\rm half}$, since usually $[P(0, L) - P(\infty, L)]/P(\infty, L) \sim e^{\mathcal{O}(L)}$ [46], it follows that

$$F_{\sigma^2}(\#) = \frac{\sigma^2(\#)(N_I, L) - \sigma^2(\#)(\infty, L)}{\sigma^2(\#)(\infty, L)} Q(\sigma^2(\#)) \sim e^{\mathcal{O}(L)} e^{-\mathcal{O}(L^{-\alpha} N_I)}. \quad (26)$$

Setting the exponents of the above relations to zero, we estimate that $N_I \sim \mathcal{O}(L^{\alpha+1})$ gates are needed to obtain chaos under (22) and (23). For the two cases whose ensuing dynamics is generic-like but not exactly GU-valued, i.e. CFF : CGU → CGU and $\mathrm{FF}_{\vert\Psi_1\rangle}$: $\mathrm{ZZ}_{\pi/4}$ → new for which $P(\infty, L) \neq P_{\rm GU}$, this holds as the condition to obtain the final generic-like dynamics. For example, for FF : GU, $\alpha \sim 1/2$ such that $N_I \sim \mathcal{O}(L^{3/2})$ gates are needed to reach GU entropy mean values.

We also confirmed existing results for the doping of CL circuits with $\mathrm{T} = \mathrm{diag}(1, e^{i\pi/4})$ and GU gates, i.e. CL : T and CL : GU, namely that $\alpha = 0$ for $\sigma^2(S)$ and $\sigma^2(S^{(2)})$, such that $\mathcal{O}(L)$ intruders are required to obtain chaos [53]. Moreover, in Ref. [46] we confirmed the scaling of the mean (normalized) ratio of level spacings $\langle \tilde{r} \rangle$ [54]: $\langle \tilde{r}_{\rm GUE} \rangle - \langle \tilde{r} \rangle \propto e^{-\beta N_I L}$. This is, in the thermodynamic limit, a single gate leads $\tilde{r}$ to become W-D distributed, which also signals a transition to a 4-design [55] but not to chaos, which restricts the error in obtaining a 4-design to scale with $e^{-\mathcal{O}(L)}$ [53]. The behaviour of $\langle \tilde{r} \rangle$ for doped FF circuits was also studied, and the results are presented in Ref. [53]: $\langle \tilde{r} \rangle$ saturates after few intruders are applied and we cannot identify its scaling with L or N_I.

Discussion. The doping of FF dynamics usually leads to chaotic dynamics, in the sense that the different measures used become GU-valued. In the presence of conservation laws − particle number for CFF : CGU and parity conservation for $\mathrm{FF}_{\vert\Psi_1\rangle}$: $\mathrm{ZZ}_{\pi/4}$ − the system also becomes generic-like, but within sectors of the conserved quantity (e.g. within sectors of fixed particle number for CGU).

The question of when chaos is reached is relative to the criteria used. One is often satisfied with obtaining a 4-design, within some error, which can reproduce the most common chaotic measures. Our results suggest that criteria (22) (used for mean values) is more restrictive than (23) (used for fluctuations), leading to higher values of α, as seen in Tab. I. Although $\mu(S^{(2)})$ and $\sigma^2(S^{(2)})$ related to conditions (22) and (23) signal 2 and 4-designs [39, 40], respectively, and the latter is harder to achieve, the conditions on the error of $\mu(S^{(2)})$ are more restrictive: to demand the mean entropies to reach the GU value within its typical error demands a higher N_I than to require the error in obtaining the fluctuations to scale at most with the GU fluctuations themselves.

Besides, different probes are more or less sensitive to chaos. In general, the mean entropies $\mu(S)$ and $\mu(S^{(2)})$ are not good probes of chaos: e.g. they are already saturated for CL circuits due to it being a 3-design [56],

although it fails to be chaotic. However, here we observe that these can identify chaos when the underlying dynamics is FF, since $S_\infty^{\rm FF} < S_{\rm Page}$ (FF circuits are not even a 1-design). Moreover, the mean ratio of level spacings for doped FF (obtained in Ref. [46]) reaches the W-D value within very few N_I (its scaling with N_I or L cannot even be identified), while the mean entropies have not yet saturated. This questions the idea that level spacing statistics is a better diagnosis of chaos than entanglement entropies and further investigation is required.

VI. CONCLUSIONS

Exact results for non-equilibrium dynamical processes are important to uncover their underlying physics and, at the same time, are scarce due to the complexity of the problem. In Section III, we have exactly computed the OTOC measuring diffusive operator spreading in a random circuit model with both number conserving (C-ST) and non-conserving quadratic fermionic terms, with (NC-ST) or without (NC-T) spatial disorder. This is in accordance with the diffusive spreading of correlations seen to occur in Hamiltonian models of quadratic fermions in 1D subjected to noise [31, 34–36]. The diffusive spreading of operators is accompanied by the diffusive growth of entanglement [14, 31, 32], as confirmed in Section IV. In the long time limit, the states resulting from FF dynamics are extended with volume law entanglement but do not explore the full Hilbert space, departing significantly from random matrix eigenstates. This contrasts with GU and CL circuits, which exhibit ballistic spreading of correlations with entanglement approaching the Page value asymptotically. All at once, these results strongly suggest that, in Hamiltonian models of free fermions, Anderson localization is destroyed by the noise we have considered and that ballistic propagation, expected for spatially homogeneous systems, becomes diffusive in the presence of noise. Although this is known to occur, an underlying physical picture for such behaviour is still elusive. We found that $\overline{\mathcal{C}(r,t)}$ for FF in a random landscape is analogous to a classical random walk, but further physical explanation is required, eventually along the lines of scattering of quasi-particles produced by circuit disorder [57]. Further study of FF dynamics doped with ZZ gates (which 'turn on' low order interactions), eventually traceable to an interacting Hamiltonian, could help clarifying the transition to the ballistic regime.

In the $N_I \to \infty$ limit, the doping of FF circuit usually results in chaotic dynamics. The scaling of several probes with system size, L, and the number of intruders, N_I, allows us to obtain bounds on the number of intruders needed to reach chaos (under conditions (22) and (23)): $N_I \sim \mathcal{O}(L^{\alpha+1})$, with α given in Tab. I for the different dynamics. The value of α depends on the underlying dynamics, on the type of intruders, on the probe used and on the conditions (22) and (23) admitted as a frontier to chaos. Since FF dynamics (not even a 1-design) are further from GU than CL dynamics (a 3-design), it is natural that higher N_I is needed to drive FF to GU: $N_I \sim \mathcal{O}(L^{1.25})$ to $\mathcal{O}(L^2)$ instead of $N_I \sim \mathcal{O}(L)$. Besides, when doping FF circuits, the presence of conserved charges slows down the crossover to the final dynamics. All at once, the number of intruders required to reach GU is extensive with system size which should indicate that, as one approaches the chaotic regime, the ability to classically simulate the dynamics is lost. So far, we know CL and FF to be integrable-like dynamics realizable with quantum circuits. By doping non-generic quantum circuits with some number of intruder gates, we find instances of intermediate dynamics between integrable-like and chaotic dynamics. This could be useful to realize lower order t-designs to obtain some chaotic valued measures, without the dynamics being fully chaotic.

Open questions remain regarding the doping of FF dynamics. The results for the bounds on N_I arise from numerical simulations, and should be strengthened by exploring higher system sizes (possibly up to $L = 20$). Besides, it would be interesting to fix these bounds by quantifying them as done in Ref. [53] for CL circuits, guaranteeing its validity in the thermodynamic limit. Another question is: what are the good measures of chaos? Although the level spacing statistics (or its normalized ration, $\tilde{r}$) is usually taken to be a better probe of chaos than mean entanglement entropies, in doped FF circuits we see instances were the contrary seems to hold. To determine the scaling of $\langle\tilde{r}\rangle$ (does the scaling $\langle\tilde{r}_{\rm GUE}\rangle - \langle\tilde{r}\rangle \propto e^{-\beta N_I L}$ valid for doped CL circuits hold for FF circuits?) and of higher moments of $\tilde{r}$ should help clarifying this.

To identify chaos in a systematic and consistent manner, future work should further explore its relation to randomness and circuit complexity: chaos can be related to a 'high enough' t-design, which can be probed using the $t^{\rm nd}$ Rényi entropy and $2t$-point OTOCs. Along these lines, it would be worth exploring the breaking of integrability by studying the effect of doping on the free fermion OTOC, both numerically and analytically. This could pass by computing the free fermion OTOC in the many-body picture and conciliating this with the analytical picture found for generic circuits in Ref. [15], which should become valid in the strong doping regime. It is possible that a light-cone could emerge when adding an intruder [54], such that we could observe the diffusive operator spreading turning into ballistic. This scenario (and, overall, the doping of circuits) should constitute a good 'laboratory' to elucidate the diffusive and ballistic regimes occurring respectively in noisy and interacting fermion models.

[1] T. Kinoshita, T. Wenger, and D. S. Weiss, Nature **440**, 900 (2006).

[2] R. Islam, R. Ma, P. M. Preiss, M. E. Tai, A. Lukin,

M. Rispoli, and M. Greiner, Nature **528**, 77 (2015).
[3] M. Cheneau, P. Barmettler, D. Poletti, M. Endres, P. Schauß, T. Fukuhara, C. Gross, I. Bloch, C. Kollath, and S. Kuhr, Nature **481**, 484 (2012).
[4] M. Gärttner, J. G. Bohnet, A. Safavi-Naini, M. L. Wall, J. J. Bollinger, and A. M. Rey, Nature Physics **13**, 781 (2017).
[5] P. Calabrese and J. Cardy, Physical Review Letters **96**, 10.1103/physrevlett.96.136801 (2006).
[6] P. Calabrese and J. Cardy, Journal of Statistical Mechanics: Theory and Experiment **2007**, P10004–P10004 (2007).
[7] C. Kollath, A. M. Läuchli, and E. Altman, Phys. Rev. Lett. **98**, 180601 (2007).
[8] A. Polkovnikov, K. Sengupta, A. Silva, and M. Vengalattore, Reviews of Modern Physics **83**, 863–883 (2011).
[9] L. D'Alessio, Y. Kafri, A. Polkovnikov, and M. Rigol, Advances in Physics **65**, 239–362 (2016).
[10] U. Schollwöck, Annals of Physics **326**, 96–192 (2011).
[11] P. Hayden and J. Preskill, Journal of High Energy Physics **2007**, 120–120 (2007).
[12] A. Kitaev, in *Talk given at the Fundamental Physics Prize Symposium*, Vol. 10 (2014).
[13] J. Maldacena, S. H. Shenker, and D. Stanford, Journal of High Energy Physics **2016**, 10.1007/jhep08(2016)106 (2016).
[14] A. Nahum, J. Ruhman, S. Vijay, and J. Haah, Phys. Rev. X **7**, 031016 (2017).
[15] A. Nahum, S. Vijay, and J. Haah, Phys. Rev. X **8**, 021014 (2018).
[16] C. W. von Keyserlingk, T. Rakovszky, F. Pollmann, and S. L. Sondhi, Phys. Rev. X **8**, 021013 (2018).
[17] V. Khemani, A. Vishwanath, and D. A. Huse, Physical Review X **8**, 10.1103/physrevx.8.031057 (2018).
[18] T. Rakovszky, F. Pollmann, and C. Von Keyserlingk, Physical Review X **8**, 031058 (2018).
[19] T. Rakovszky, F. Pollmann, and C. W. von Keyserlingk, Phys. Rev. Lett. **122**, 250602 (2019).
[20] A. I. Larkin and Y. N. Ovchinnikov, Soviet Journal of Experimental and Theoretical Physics **28**, 1200 (1969).
[21] P. Hosur, X.-L. Qi, D. A. Roberts, and B. Yoshida, Journal of High Energy Physics **2016**, 4 (2016).
[22] V. Khemani, D. A. Huse, and A. Nahum, Phys. Rev. B **98**, 144304 (2018).
[23] S. Sachdev and J. Ye, Physical Review Letters **70**, 3339–3342 (1993).
[24] A. Kitaev, in *KITP strings seminar and Entanglement*, Vol. 12 (2015) p. 26.
[25] D. N. Page, Phys. Rev. Lett. **71**, 1291 (1993).
[26] P. Calabrese and J. Cardy, Journal of Statistical Mechanics: Theory and Experiment **2005**, P04010 (2005).
[27] M. Žnidarič, Communications Physics **3**, 10.1038/s42005-020-0366-7 (2020).
[28] Y. Huang, IOP SciNotes **1**, 035205 (2020).
[29] J. H. Bardarson, F. Pollmann, and J. E. Moore, Phys. Rev. Lett. **109**, 017202 (2012).
[30] M. Serbyn, Z. Papić, and D. A. Abanin, Phys. Rev. Lett. **110**, 260601 (2013).
[31] G. Roósz, R. Juhász, and F. Iglói, Phys. Rev. B **93**, 134305 (2016).
[32] X. Cao, A. Tilloy, and A. D. Luca, SciPost Phys. **7**, 24 (2019).
[33] D. Bernard and T. Jin, Phys. Rev. Lett. **123**, 080601 (2019).
[34] D. Bernard and T. Jin, arXiv preprint arXiv:2006.12222 (2020).
[35] S. Nandy, A. Sen, and D. Sen, Phys. Rev. X **7**, 031034 (2017).
[36] J. Marino and A. Silva, Phys. Rev. B **86**, 060408 (2012).
[37] J.-S. Caux and J. Mossel, J. Stat. Mech. Theory Exp. **2011**, P02023 (2011).
[38] D. Gross, K. Audenaert, and J. Eisert, Journal of Mathematical Physics **48**, 052104 (2007).
[39] D. A. Roberts and B. Yoshida, Journal of High Energy Physics **2017**, 10.1007/jhep04(2017)121 (2017).
[40] Z.-W. Liu, S. Lloyd, E. Y. Zhu, and H. Zhu, Physical Review Letters **120**, 10.1103/physrevlett.120.130502 (2018).
[41] L. G. Valiant, SIAM Journal on Computing **31**, 1229 (2002).
[42] B. M. Terhal and D. P. DiVincenzo, Phys. Rev. A **65**, 032325 (2002).
[43] F. Mezzadri, arXiv preprint math-ph/0609050 (2006).
[44] D. Gottesman, arXiv preprint quant-ph/9807006 (1998).
[45] E. Lieb, T. Schultz, and D. Mattis, Annals of Physics **16**, 407 (1961).
[46] Dias B. C., MSc thesis (2021).
[47] P. W. Anderson, Phys. Rev. **109**, 1492 (1958).
[48] Y. Huang, IOP SciNotes **1**, 035205 (2020).
[49] J. M. Magán, Phys. Rev. Lett. **116**, 030401 (2016).
[50] C. Liu, X. Chen, and L. Balents, Phys. Rev. B **97**, 245126 (2018).
[51] D. Bernard and L. Piroli, Entanglement distribution in the quantum symmetric simple exclusion process (2021), arXiv:2102.04745 [cond-mat.stat-mech].
[52] P. Łydżba, M. Rigol, and L. Vidmar, Phys. Rev. Lett. **125**, 180604 (2020).
[53] L. Leone, S. F. Oliviero, Y. Zhou, and A. Hamma, arXiv preprint arXiv:2102.08406 (2021).
[54] S. Zhou, Z. Yang, A. Hamma, and C. Chamon, SciPost Physics **9**, 10.21468/scipostphys.9.6.087 (2020).
[55] J. Haferkamp, F. Montealegre-Mora, M. Heinrich, J. Eisert, D. Gross, and I. Roth, arXiv preprint arXiv:2002.09524 (2020).
[56] H. Zhu, Physical Review A **96**, 10.1103/physreva.96.062336 (2017).
[57] D. Bernard and B. Doyon, Physical Review Letters **119**, 10.1103/physrevlett.119.110201 (2017).